



Universiteit
Leiden
The Netherlands

Plasmonic enhancement of one-photon- and two-photon-excited single-molecule fluorescence by single gold nanorods

Zhang, W.

Citation

Zhang, W. (2018, June 27). *Plasmonic enhancement of one-photon- and two-photon-excited single-molecule fluorescence by single gold nanorods*. *Casimir PhD Series*. Retrieved from <https://hdl.handle.net/1887/62864>

Version: Not Applicable (or Unknown)

License: [Licence agreement concerning inclusion of doctoral thesis in the Institutional Repository of the University of Leiden](#)

Downloaded from: <https://hdl.handle.net/1887/62864>

Note: To cite this publication please use the final published version (if applicable).

Cover Page



Universiteit Leiden



The handle <http://hdl.handle.net/1887/62864> holds various files of this Leiden University dissertation

Author: Zhang, Weichun

Title: Plasmonic enhancement of one-photon- and two-photon-excited single-molecule fluorescence by single gold nanorods

Date: 2018-06-28

2

Plasmonic enhancement of a near-infrared fluorophore using DNA transient binding

Fluorescence enhancement by plasmonic nanostructures enables the optical detection of single molecules with weak fluorescence, extending the scope of molecular fluorescence imaging to new materials and systems. In this work, we make use of the reversible hybridization of fluorophore-carrying short DNA oligomers to their complementary docking strands (immobilized on the surface of gold nanorods or the glass substrate) to visualize single-molecule enhancement events near individual gold nanorods. Docking strands attached to the glass substrate are found to be more photo-stable. We find over 3,000-fold fluorescence enhancement of single molecules of IRDye800CW, a near-infrared dye with a low quantum yield of 7%. This strong enhancement, consistent with numerical simulations, arises from the combined effect of local field enhancement and the competition between radiative and nonradiative decay rate enhancements.

2.1. Introduction

Noble metal nanoparticles of various morphologies have been at the center of research (see reviews [1–6] and references therein) because of their remarkable optical properties derived from their localized surface plasmons. A wealth of applications based on plasmonic nanoparticles have been explored, such as imaging [7], (bio-)sensing [8], and photothermal therapy [9–11]. The strong local fields generated around nanoparticles upon resonant excitation can modify the interaction of neighbouring molecules with light, giving rise to diverse applications such as surface-enhanced Raman spectroscopy [12, 13] and metal-enhanced fluorescence [14–19].

In metal-enhanced fluorescence, plasmonic nanoparticles can be described as optical nano-antennas interacting strongly with fluorophores, enhancing their excitation and radiative rates, and opening new non-radiative dissipation channels (quenching), and consequently influencing their fluorescence emission [14, 15, 20]. Fluorescence enhancement of fluorophores emitting at wavelengths in the near-infrared region is of particular interest. Due to the absence of autofluorescence and deeper penetration depth under near-infrared excitation, near-infrared dyes have extensive *in vivo* applications in biosensing and molecular fluorescence bioimaging [21, 22]. Unfortunately, most biocompatible near-infrared-emitting dyes (*e.g.* Indocyanine Green) are weak fluorophores with low quantum yields [23]. Gold nanoparticles have been used to enhance the fluorescence brightness of near-infrared-emitting fluorophores by two orders of magnitude, improving significantly the detection limits of near-infrared fluorescence imaging [24–27]. At the single-molecule level, the enhancement is more pronounced because of the absence of ensemble averaging over many molecules, most of which are not in the plasmonic hot spots. If a single fluorophore is placed in the right position, plasmonic nanoparticles can enhance its fluorescence by two to four orders of magnitude upon radiation with a resonant laser [28–30]. Herein, we demonstrate that plasmonic nanoparticles enable sensitive detection of near-infrared fluorophores, even at the single-molecule level.

One of the major difficulties of studying single molecules by fluorescence enhancement is the accurate positioning of the molecule of interest with respect to the nanostructures at the nanometer scale. Different approaches were proposed, including slow free diffusion [31], non-specific transient sticking [29, 32, 33], and immobilization of single molecules [28, 30, 34–36]. The observation time of single molecules for diffusion and immobilization methods is often limited. Diffusion times in the near field are often shorter than 1 ms, making it difficult to study slower dynamics and to detect fluorescence enhancement with low photon rates. While molecules can be immobilized almost permanently close to the nanoantennas, the observation time is limited by photobleaching. Consequently, each nanoantenna can be studied with only one or a few molecules at best.

Transient binding approaches offer an elegant solution for the photobleaching problem while giving a reasonable observation time. However, non-specific sticking is dependent on many factors including the properties of the diffuser, the surrounding medium, as well as the surface conditions of the substrate, leading to an unpredictable sticking time. Here we make use of the sequence-specific and reversible hybridization of complementary DNA strands to study the fluorescence enhancement of single molecules of a near-infrared dye by an individual plasmonic nanostructure. DNA hybridization offers a reliable, reproducible and

controllable mechanism for transient binding thanks to highly predictable base pairing and binding energy [37]. Reversible hybridization of short DNA strands facilitates the targeting of the surface of objects by diffusing fluorescent probes, which is the key principle of a super-resolution imaging technique known as DNA-PAINT [38–40] (points accumulation for imaging in nanoscale topography).

Similar to the idea of DNA-PAINT, we use the transient binding and dissociation of short dye-labeled DNA strands (“imager strand”) in solution to their complementary target strands (“docking strands”) immobilized either on the surface of gold nanorods or the glass substrate to bind fluorescent molecules in the hot spot of a nanostructure. In contrast to immobilizing fluorophores, the DNA-based strategy is limited by photobleaching because photobleached molecules are continuously replenished with fresh ones. Furthermore, the binding time of the imager strand to the docking strand can be adjusted by the electrolyte concentration, the number of complementary base pairs and the temperature. The chemistry and kinetics of DNA hybridization have been extensively characterized [38, 41].

The selected plasmonic nanostructure for our study is individual gold nanorods. Such nanoparticles are widely explored for several applications such as plasmonic sensing [3, 42], nanoheating [43] and for fluorescence enhancement [29, 44], as they offer narrow and tunable surface plasmon resonances (SPR) from the visible to the near-infrared “water window”. They also provide highly confined nanometric volumes with easy access for molecules near their tips. Gold surfaces can be readily functionalized with thiolated molecules, taking advantage of the strong Au-S bond. Moreover they are easy to fabricate with wet-chemical methods and they can be used in solution, without the need of a supporting substrate.

We studied two different approaches to enhance the fluorescence of single molecules using DNA transient binding. i). The docking DNAs are immobilized on the nanorod surface; ii). The docking DNAs are immobilized to the glass substrate surface. We characterized the enhancement factors, the binding times, and the photo-stability. We found a maximum enhancement factor of 3,500-fold, which is in good agreement with numerical calculations.

2.2. Materials and methods

IRDye800CW molecules were used for the enhancement study. An IRDye800CW molecule is conjugated to a short oligonucleotide strand of 10 base pairs (Integrated DNA Technologies, Inc.). IRDye800CW is a near-infrared dye with a low quantum yield of 7% [25]. The absorption maximum of the imager construct (DNA plus dye) is observed at 780 nm, and the fluorescence emission maximum appears at 796 nm in HEPES buffer (Fig. 2.1(a)).

Attachment of docking strands. Clean coverslips were first functionalized with (3-mercaptopropyl)trimethoxysilane to create a thiol-terminated surface. Individual gold nanorods were adsorbed onto the functionalized surface from a dilute aqueous suspension of gold nanorods (Nanopartz Inc.). The resulting density of nanorods was limited to $6/(100 \mu\text{m}^2)$ so that there was only one nanorod in the focus of the fluorescence microscope. The average size of the nanorods was $38 \text{ nm} \times 118 \text{ nm}$ by diameter and length. This size was chosen such that the longitudinal plasmon resonance overlaps well with both the excitation wavelength and the emission wavelength of the dye (Fig. 2.1(b)), ensuring a high fluorescence enhancement factor [29, 44].

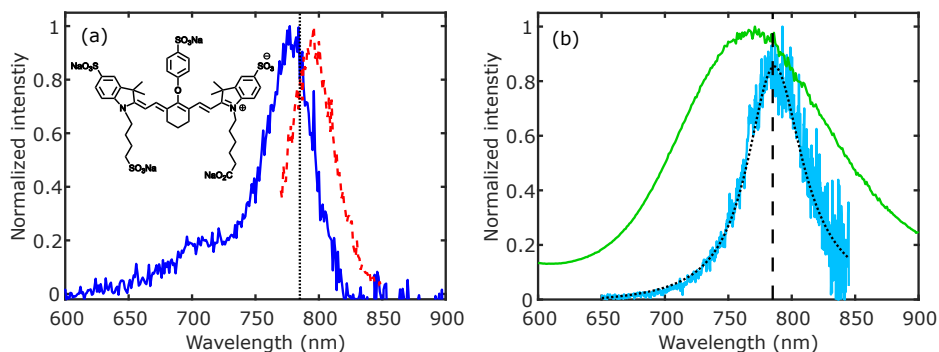


Figure 2.1: **Spectra of IRDye800CW and gold nanorods.** (a) Absorption and emission spectra of IRDye800CW conjugated with the imager DNA strand in HEPES buffer are shown as the blue solid line and red dashed line, respectively ($\lambda_{\max-\text{abs}} \sim 780$ nm, $\lambda_{\max-\text{em}} \sim 796$ nm). The absence of the shoulder in the emission spectrum corresponding to the vibronic absorption band is attributable to the low near-infrared response of the spectrofluorometer. Inset: chemical structure of IRDye800CW. (b) The green line shows the bulk extinction spectrum of gold nanorods used in this work dispersed in water. The extinction maximum was observed at 771 nm. The broad extinction band stems from the size distribution of nanorods in the suspension. The light blue curve shows the photoluminescence spectrum of a single gold nanorod. The spectrum is corrected for the wavelength-dependence collecting efficiency of the setup and fitted with a Lorentzian line shape (black dotted line), yielding a resonance wavelength of 786.4 ± 0.4 nm. The wavelength of the excitation laser (785 nm) is represented by the dashed vertical lines in the plots.

Docking DNA strands were attached, either onto the nanorod surfaces or the glass substrate, as described in detail in the Supporting Information. Briefly, to functionalize the nanorod surface with docking strands, the nanorod-loaded coverslips were treated with dithiol-derived oligonucleotides and thiol-derived polyethylene glycol (PEG-SH). The oligonucleotide contains dithiol phosphoramidite at one terminus and 15 base pairs, 10 of which are complementary to those of the imager strand. Both the oligonucleotides and PEG chains can bind to the nanorods. The ratio of docking strands and PEG molecules was kept at around 1 : 1000 to ensure only single or a few docking strands at the tips of a nanorod. The coverslip surface was further covered with bovine serum albumin (BSA) using 4-(p-maleimidophenyl)butyrate (SMPB) as a cross-linker to minimize non-specific adsorption of the fluorophores on the surface.

To functionalize the coverslip surface with docking strands, a layer of NeutrAvidin molecules was attached to the coverslips with gold nanorods using SMPB as the linker. Biotin-terminated docking strands were then tethered to the substrate via biotin-NeutrAvidin interactions. The docking strand contains 20 base pairs, 10 of which are complementary to those of the imager strand. The coverslip surface was thus saturated with docking DNA strands that could hybridize with the imager strands while the nanorod surface had no docking strands attached. See the Supporting Information for the details of sample preparation.

Confocal microscopy. Single-molecule fluorescence enhancement studies were performed on a home-built sample-scanning microscope at room temperature. A linearly polarized diode laser (785 nm, continuous-wave, Toptica Photonics) or a circularly polarized 532-nm continuous-wave laser (532 nm, continuous-wave, Shanghai Laser & Optics Cen-

ture Co., Ltd) was reflected by a 10/90 beam splitter into an oil immersion objective (100 \times , NA=1.4, Zeiss) to excite the dye molecules or to measure the photoluminescence spectra of gold nanorods. Emission from the focal volume was collected by the same objective and transmitted by the beam splitter. After the scattered light from the excitation laser was filtered out by suitable notch filters, fluorescence was focused on a multi-mode optical fiber with a core of 62 μm in diameter. The optical fiber is equivalent to a confocal pinhole. The output of the optical fiber was detected by an avalanche photodiode (SPCM-AQR-16, PerkinElmer). The setup was equipped with a spectrometer with a liquid-nitrogen-cooled CCD (Acton SP-500i, Princeton Instruments). The photoluminescence spectra were corrected for the low near-infrared response of the optics (Fig. S2.2, Supporting Information). Figure 2.1(b) shows the photoluminescence spectrum of a single gold nanorod, which shows a narrow Lorentzian spectral shape. Thus aggregates of nanoparticles can be easily recognized and excluded from further studies [45].

2.3. Results and discussion

2.3.1. Binding sites on the nanorod surface

Thiolated docking DNA strands were tethered to the surface of gold nanorods together with thiolated competitor molecules to regulate the density of binding sites. The concentration of dye-labeled imager strand was 100 nM with 500 mM NaCl in HEPES pH 7.0 buffer. NaCl provides the necessary ion strength required for the desired DNA-binding kinetics. The distance between the chromophore and nanorod surface is set by the number of base pairs in the DNA docking-imager construct. We estimated a total distance of 4 nm using an inter-base pair distance of 0.33 nm and considering the length of the linker to the gold surface.

When the 785-nm laser was focused on the individual immobilized nanorods, we recorded fluorescence time traces, which showed fluorescence bursts corresponding to transient hybridization of the imager strand to the docking strands immobilized near the tips of the nanorod. The excitation was kept at a very low power (2 nW) to minimize photobleaching of the dye molecules while detecting enough fluorescence intensity to identify transient enhancement events of single molecules.

Since the competition of binding to the gold surface between the docking strands and competitor molecules is a random process, the number and position of docking strands on the nanorod surface vary from nanorod to nanorod. Therefore, fluorescence bursts with different intensity levels may be identified on the time traces taken on different nanorods. Figure 2.2(b) shows a time trace with only one observable docking site. In such a scenario, many refreshing single molecules can be studied *at the same* position in the plasmonic hot spot, evidenced by the stable high level intensity measured. Every binding site can be measured, in theory, over unlimited period of time. This opens the study of different kinds of single molecules in the same nanoscale environment with significant statistics. With such an experimental scheme, a rich variety of single-molecule studies can be envisioned. One such example is to study the enhancement factors for molecules with different quantum efficiencies with great control over their positions with respect to plasmonic nanostructures.

The binding time of the imager to the docking strands depends on many factors including

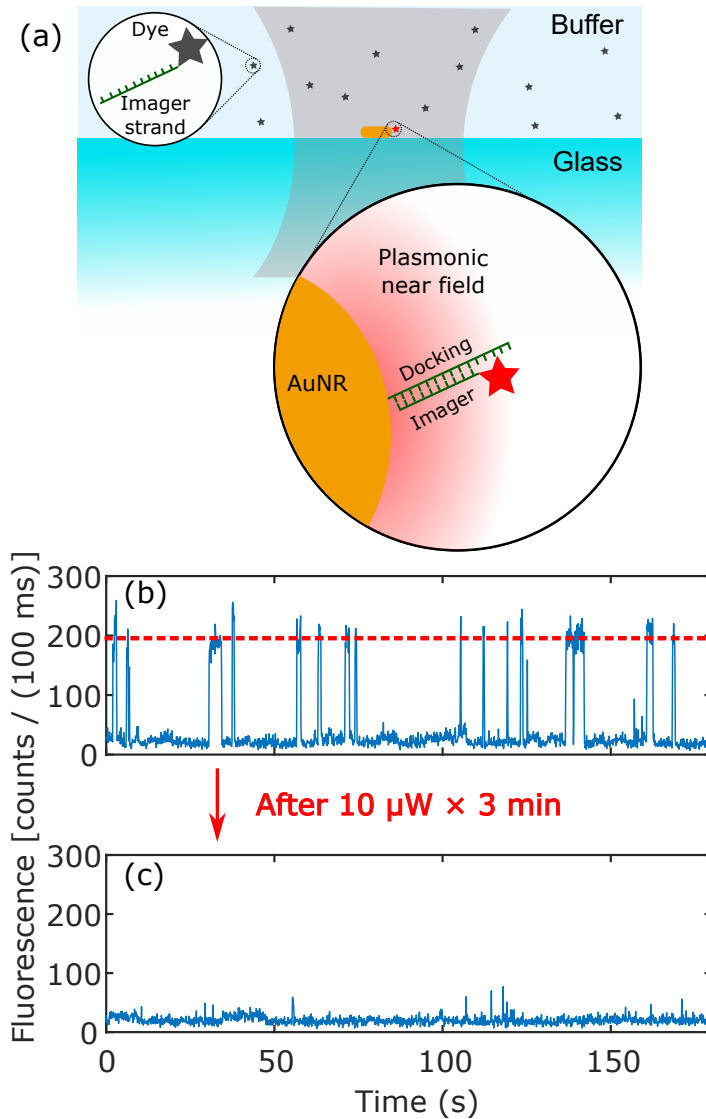


Figure 2.2: **Fluorescence enhancement with the docking strands on the nanorods.** (a) Schematic of transient binding. Immobilized nanorods are functionalized with docking strands. The imager-IRDye800CW strands in the solution are shown as gray stars representing unenhanced fluorescence. One of the imagers is hybridizing to a docking strand attached to the tip of the nanorod and is shown as a red star representing plasmon-enhanced fluorescence emission. (b) Typical time trace with one observable docking site (intensity height indicated by the red dashed line) taken on a nanorod under an excitation of a 2-nW, 785-nm laser. After irradiating by the same laser with $10 \mu\text{W}$ for 3 minutes, the nanorod no longer shows fluorescence bursts, indicating that the docking strand is no longer operational. (c) Time trace taken on the same nanorod shown in (b) after the high-power laser irradiation. There is no observable docking site.

the number of complementary base pairs, the salt concentration, and the temperature. The average burst duration of the fluorescence bursts in Fig. 2.2(b) is 0.93 ± 0.36 s. A long binding time is favorable for collecting enough photons to identify single molecule enhancement events, particularly when the fluorescence count rate is low. Jungmann *et. al.* reported an average bound time of 5 s for a duplex length of 10 base pairs at similar conditions [38], which is in agreement with the order of magnitude we obtained here. We attribute the small difference to photobleaching and blinking of the fluorophores.

The weak background in Fig. 2.2(b), ~ 20 counts in 100 ms, comes from the detector's dark counts, from all the fluorescent molecules in the focal volume of the excitation laser as well as from some photoluminescence of the gold nanorod. The average intensity of the fluorescence bursts is 200 counts in 100 ms, corresponding to a count rate of 1,800 counts/s from a nanorod-enhanced IRDye800CW molecule excluding the background. To quantify the fluorescence enhancement, we measured the average count rate from a molecule when not enhanced by measuring the size of the focal volume and the count rate from all the molecules in it, as described in the Supporting Information. These measurements yielded a molecular brightness of 2.0 ± 0.3 counts/s/molecule. Therefore, the bursts in Fig. 2.2 (b) correspond to an enhancement factor of 900.

Concerned with the stability of the transient binding, we deliberately applied high laser power to the nanorods and found that transient binding events typically disappear under continuous irradiation of some μW for a few minutes. For example, after measuring trace of Fig. 2.2(b) we irradiated the nanorod with the 785-nm continuous-wave laser at $10 \mu\text{W}$ for 3 minutes. We then measured again with low power and found no DNA-binding events, as shown in Fig. 2.2(c). The remaining short and low-intensity events are attributed to unspecific sticking to the glass surface as found previously [29, 32].

We then aim to explore the possible reasons for the disappearance of the bursts. Firstly we consider a perturbation of the hybridization equilibrium due to an increased local temperature due to plasmonic heating of the nanorod [43]. We estimated the surface temperature of the nanorod under the illumination conditions used in this work and found an increase of 5.3 K with a laser power of $10 \mu\text{W}$ (Supporting Information). It appears that the docking strand was permanently removed or damaged by irradiation of high laser intensity, namely, the reactivity of the base pairs on the docking strand was lost or the gold-thiol bond was broken, followed by the release of the entire docking strand. Light-induced breaking of gold-thiol bond in such a nanoparticle-DNA system has been observed under irradiation of pulsed lasers, and is usually attributed to the excitation of hot electrons at the surface of the nanoparticle [46, 47]. Continuous-wave lasers were only observed to affect dehybridization of DNAs by photothermally increasing the bulk temperature of the solution. However, the intensity of resonant irradiation we applied (8.8 kW/cm^2) was at least three orders of magnitude higher than previous bulk measurements [46, 48]. Thus, our conditions generate much more hot electrons, resulting in enhanced photo-induced reactions and hence the loss of docking strands attached to the gold surface.

To further test this hypothesis, we investigated nanorods with multiple observable docking strands. We found that docking strands associated with higher enhancement were generally more vulnerable to laser illumination. Figure 2.3(a) shows a time trace from a nanorod with two observable docking sites (recorded with an excitation power of 2 nW), evidenced by the fluorescent bursts with two distinct heights. After increasing the laser power to 10

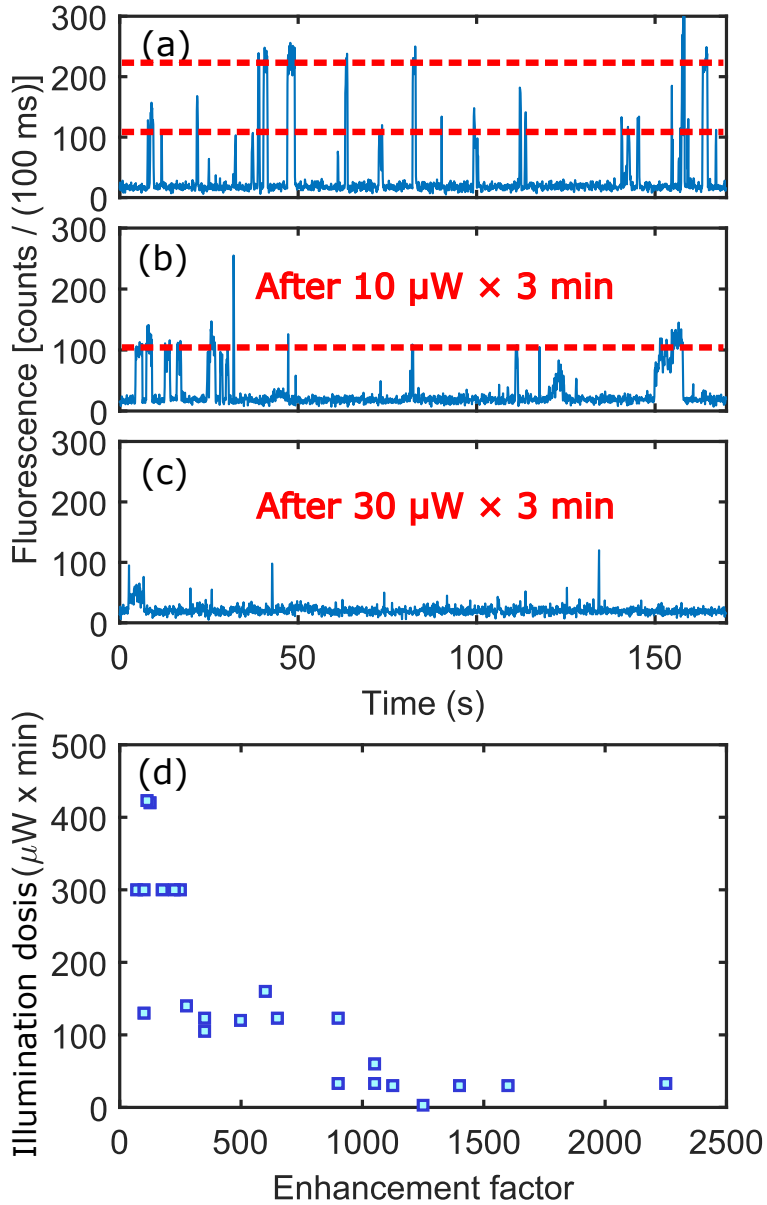


Figure 2.3: (a-c) Fluorescence time traces taken on the same gold nanorod at an excitation power of 2 nW. The original time trace (a) shows 2 observable binding sites (indicated by the red dashed lines). (b) After irradiating with the same laser at $10 \mu\text{W}$ for 3 minutes, the fluorescence bursts with higher enhancement have disappeared. (c) After irradiating at $30 \mu\text{W}$ for another 3 minutes, fluorescence bursts with lower enhancement also disappear. (d) Negative correlation between the enhancement factor that each docking site produces and the "dose of irradiation" that was applied before it was completely damaged.

μW and irradiating for 3 minutes, the time trace measured at 2 nW showed only one observable binding site (Fig. 2.3(b)). The only short and high burst is attributable to non-specific sticking of imager strands to the substrate near the nanorod. We further increased the laser power to 30 μW and irradiated for another 3 minutes, after which the nanorod showed no transient binding at all (Fig. 2.3(c)).

Further examination of more nanorods showed that the breaking of docking sites is also dependent on the duration of irradiation. We define the product of the laser power and irradiation time as the "illumination dose" and correlate the enhancement factor that each docking site produces with the dose of irradiation that was applied before it was completely damaged, as shown in Fig. 2.3(d). Although the applied dose of irradiation should be higher than the real threshold of photo-damage, we see a general correlation between higher enhancement factor and lower applied irradiation dose.

Our observations cannot be explained by DNA-melting since the disappearance is irreversible. The mechanism behind this irreversible disappearance cannot be laser-induced heating of the nanorod since the steady-state temperature distribution is uniform over the entire gold nanorod due to the high thermal conductivity of gold [49]. Thus, we attribute this irreversible breakage of the DNA-transient binding to hot electrons damage of the Au-S bonds.

2.3.2. Binding sites on the substrate

In a second approach, the substrate surface was saturated with docking strands. The concentration of dye-labeled imager strand was 5 nM with 500 mM NaCl in HEPES pH 7.0 buffer, as shown schematically in Fig. 2.4(a). If a dye-labeled imager strand binds to a docking strand near a gold nanorod, we see a fluorescence burst in the time trace, as shown in the upper panel of Fig. 2.4(b). The excitation power was also 2 nW. The photoluminescence spectrum of this nanorod shows a plasmon resonance at 786 nm, as shown in Fig. 2.1(b). Imager strands bind to different docking strands at random positions in the near-field, giving rise to fluorescence bursts with different intensities.

We irradiated the nanorod with increasing laser intensity and tested the presence of transient binding by measuring time traces with low laser intensity afterwards, in the same way as for the first approach. The lower panel of Fig. 2.4(b) shows the time trace recorded at 2 nW after the nanorod was irradiated under 100 μW for 3 minutes. Imager strands are still binding to the docking strands and producing long fluorescent bursts. The possible reason is that, unlike in the first approach, hot electrons generated on the surface of nanorods cannot reach the molecules that are immobilized on the substrate surface or the hot electrons cannot break the bond between the glass and the DNA docking strand.

The strongest fluorescent burst in Fig. 2.4(b) shows a count rate of ~ 7100 counts/s against a background fluorescence of ~ 200 counts/s, yielding a fluorescent enhancement factor of 3,500. This is a $4 \times$ higher enhancement than the one found in the case of the DNA docking strand was attached to the gold nanorod. We attribute this to the higher spatial sampling of the plasmonic near field in the case of the DNA attached to the glass, since we saturated the glass surface with docking strands. In the case of the docking bound to the gold surface we have a few docking sites thus it is unlikely it will be at the best enhancement position.

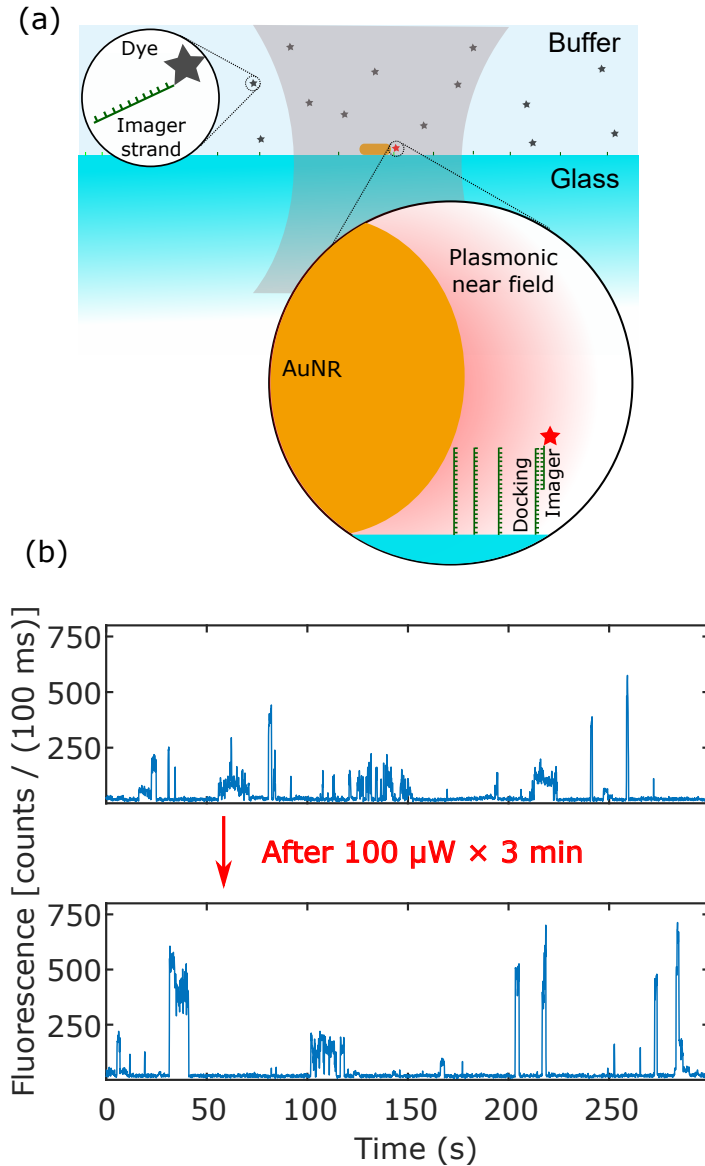


Figure 2.4: **Fluorescence enhancement with the docking strand on the coverslip surface.** (a) Schematic of transient binding. The entire glass substrate is functionalized with docking strands. The imager-IRDye800CW strands in the solution are shown in gray representing unenhanced fluorescence. One of the imagers is hybridizing to a docking strand tethered to the substrate in the near field of the nanorod and is shown in red representing plasmon-enhanced fluorescence emission. (b) The upper panel shows a fluorescence time trace taken on a nanorod under a 2-nW, 785-nm illumination. After irradiated under the same laser with 100 μ W for 3 minutes, the nanorod still produces intense fluorescence bursts.

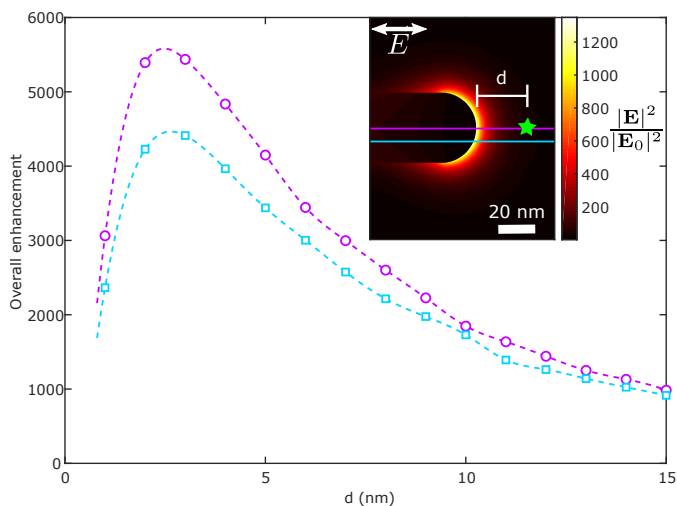


Figure 2.5: Calculated overall fluorescence enhancement factor as a function of the distance between the nanorod and an IRDye800CW molecule, d , for two different heights, as shown in the near-field map in the inset. The size of the nanorod is $38 \text{ nm} \times 116 \text{ nm}$, associated with a surface plasmon resonance wavelength of 784 nm in water.

2.3.3. Numerical simulations

We performed numerical simulations using a finite-element method (Comsol Multiphysics) and a boundary element method (SCUFF-EM) [50, 51] to understand the experimentally observed fluorescence enhancement. The details of the simulations is outlined in the Supporting Information. The nanorod in the simulation has a size of $38 \text{ nm} \times 116 \text{ nm}$. The calculated longitudinal surface plasmon resonance of the nanorod is 784 nm in water, providing a good spectral match with the excitation wavelength. We assume that the molecule is placed along the revolution axis of the nanorod. The polarization of the incident plane wave and the transition dipole moment of the molecule are parallel to the long axis of the nanorod. These settings are certainly not always valid in the experiments, but we used them to calculate the largest possible fluorescence enhancement. Figure 2.5 shows the overall enhancement factor as a function of distance between an IRDye800CW molecule and a nanorod. The optimum distance is about 4 nm to obtain the maximum fluorescence enhancement. If the molecule is too close, fluorescence quenching due to additional nonradiative decay pathways becomes dominant (Fig. S2.5) and the overall enhancement decreases; for longer distances, fluorescence enhancement diminishes because of a weaker electromagnetic field. Despite the presence of fluorescence quenching, a high maximum fluorescence enhancement factor of over $5,000$ is expectable if the molecule is aligned properly with respect to the gold nanorod, which is in line with the experimentally observed enhancements, considering the isotropic distribution of molecular dipole moments.

2.4. Conclusions and outlook

In summary, we have demonstrated the fluorescence enhancement of near-infrared emitting single molecules by individual gold nanorods thanks to their intense localized fields close to the rod tips. A DNA-based transient binding method is implemented to transiently tether single fluorescent molecules in the plasmonic near field for approximately 1 s. Binding and unbinding of short DNA strands were directly visualized thanks to enhanced fluorescence. Any molecular dynamics that leads to a fluorescence intensity change from the labeled fluorophore within the binding time could also be visualized near the nanorods. Transient binding disappears upon irradiation of strong laser intensity if the docking strands are attached to the surface of the gold nanorods through Au-thiol bonds, probably due to hot electron induced DNA release. It is therefore advised to immobilize the docking strands on the glass substrate to prevent DNA release, especially when a pulsed laser is used.

Using the strategy of immobilizing the docking strands on the glass substrate, a remarkable 3,500-fold enhancement in fluorescence intensity from single molecules was observed, which agrees well with numerical simulations. This drastic increase in fluorescence intensity is potentially valuable for enhancing the detection sensitivity and contrast of molecular bioimaging. The position of the emitter and the duration of the emitter-plasmon interaction can be manipulated by proper DNA engineering. The experimental methods presented here can be readily extended to other dyes and nanostructures.

2.5. Supporting information

2.5.1. Sample preparation

Materials. Methanol (99.8%), 3-Mercaptopropyl trimethoxysilane (MPTS, 95%), cysteamine (98%), 4-(2-Hydroxyethyl) piperazine-1-ethanesulfonic acid (HEPES, 99.5%), bovine serum albumin (BSA, 96%), tris(2-carboxyethyl) phosphine hydrochloride (TCEP, 98%) were purchased from Sigma-Aldrich; Sodium acetate (CH₃COONa, 99%) from Merck; NeutrAvidin (NA) protein and succinimidyl 4-(p-maleimidophenyl)butyrate (SMPB) from ThermoFisher. HEPES buffer (10 mM) was prepared by dissolving HEPES in milli-Q water and the pH was adjusted to 7. Acetate buffer (pH 4) was prepared from acetic acid and sodium acetate. All the DNA oligonucleotides including the single strand DNA labeled with IRDye800CW (imager-IRDye800CW) were purchased from Integrated DNA Technologies, Inc. The sequence of imager-IRDye800CW is 3'-TAT GTA GAT C-5'-IRDye800CW. Gold nanorods were purchased from Nanopartz Inc. (A12-40-780-CTAB). The average size is 38 nm × 118 nm by diameter and length.

Silanization of the coverslip surface. Glass coverslips (Menzel-Gläser, $\phi = 25$ mm, No. 1) were cleaned and silanized before further functionalization. The coverslips were sonicated in water (20 min) and ethanol (20 min). They were dried with a clean nitrogen flow and then immersed for 30 minutes with gentle stirring in a methanol solution containing 1% (3-mercaptopropyl)trimethoxysilane (Sigma-Aldrich) and 5% glacial acetic acid in a Teflon incubator. Thereafter, the silanized slides were washed thoroughly with methanol and dried with a nitrogen flow. This results in binding of the silane groups to the active hydroxyl groups and creates a thiol surface that can be used for conjugation with gold nanorods and

for passivation of the substrate surface. If not immediately used for the next step, they were stored inside a desiccator to maintain the activity of the thiol groups.

Gold nanorod immobilization. The suspension of gold nanorods we purchased is stabilized with cetyl trimethyl ammoniumbromide (CTAB). In order to immobilize the nanorods on a thiolated glass surface, we decreased the concentration of CTAB by centrifugation and resuspension in milliQ. This solution of nanorods was in contact for with the thiol-activated glass coverslip for 30 minutes. Unbound gold nanorods were washed away with milliQ water. This procedure resulted in around 6 isolated single gold nanorods per $100 \mu\text{m}^2$ area immobilized on the substrate.

Docking DNA on gold nanorods. The coverslip with gold nanorods was treated with a mixture of thiolated docking DNA strands, methoxy-poly(ethylene glycol)-thiol (mPEG7-SH, MW = 350), 5 mM NaCl and 1 mM Tris(2-carboxyethyl)phosphine hydrochloride (TCEP) in 0.1 M acetate buffer at pH = 4. The sequence of the docking strand was DTPA-5'-ATA CAT CTA GAA ATT-3'. DTPA represents dithiol phosphoramidite, which strongly binds the docking strands to the gold nanorods. The average number of docking strands on a gold nanorod can be controlled by the concentration ratio between docking strands and mPEG7-SH, which was kept at around 1:1000 to ensure only a few docking strands sat at the tips of a nanorod. TCEP was used to prevent the formation of disulfide bonds and thus maintain the reactivity of thiol groups. The incubation lasted overnight and the coverslip was washed extensively with HEPES buffer.

To prevent nonspecific sticking of imager strands to the surface, the rest of the glass surface was passivated with bovine serumalbumin (BSA). This was achieved by incubating the coverslips with 1 mM succinimidyl 4-(p-maleimidophenyl)butyrate (SMPB), 20 μM BSA and 1 mM TCEP in HEPES buffer for 2 hours. SMPB is a cross-linker that contains an amine-reactive end (N-hydroxysuccinimide ester) and a thiol-reactive end (maleimide), thereby binding BSA to the substrate. The unreacted chemicals were removed by washing with HEPES buffer. The functionalized coverslip was used immediately or stored in HEPES buffer. The chemical structure used for this situation is shown in Fig. S2.1(a).

Docking DNA on a glass substrate. The coverslip with gold nanorods was treated with 100 μM cysteamine and TCEP in 0.1 M acetate buffer at pH = 4 for at least 2 hours to passivate the surface of nanorods. After the slide was washed with HEPES buffer, it was treated with a solution with 1 μM NeutrAvidin (NA), 10 μM SMPB and 1 mM TCEP in HEPES buffer (pH = 7). SMPB is a cross-linker that immobilizes NA protein molecules onto the glass substrate. The incubation lasted 90 min and excess reagents were washed away by HEPES buffer. Lastly, 100 nM docking DNA strand in HEPES buffer was applied to the coverslip. The sequence of the docking strand was biotinTEG-5'-A GCT ATA TTT ATA CAT CTA G-3'. Biotin-TEG increases the oligo-biotin distance to 15 atoms using a triethyleneglycol (TEG) spacer. The biotinylated oligonucleotides binds strongly to the NeutrAvidin molecules. After 30 minutes, the coverslip was washed with HEPES buffer. The functionalized coverslip was used immediately or stored in HEPES buffer. The chemical structure used for this situation is shown in Fig. S2.1(b).

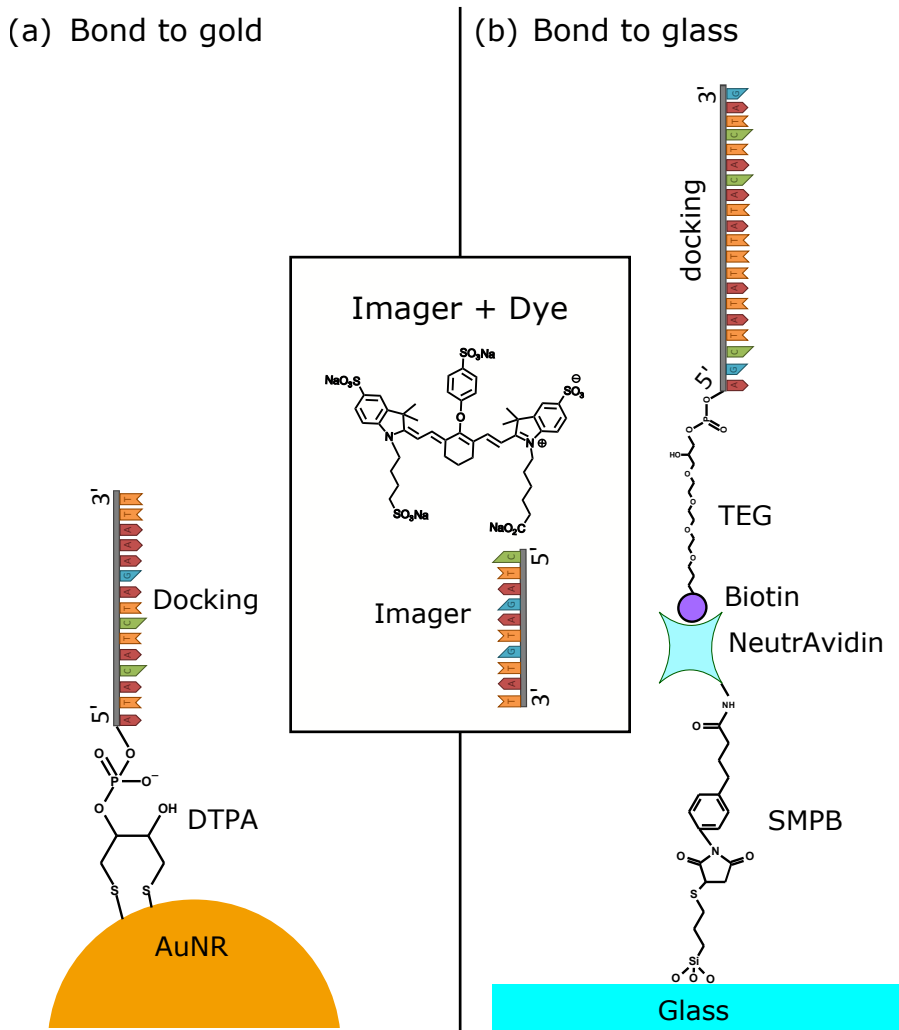


Figure S2.1: Schematic representation of the bonds used to attach the docking strand to the gold surface (a) and glass surface (b). The inset in the middle shows the imager DNA strand and the dye structure, which is the same for both cases.

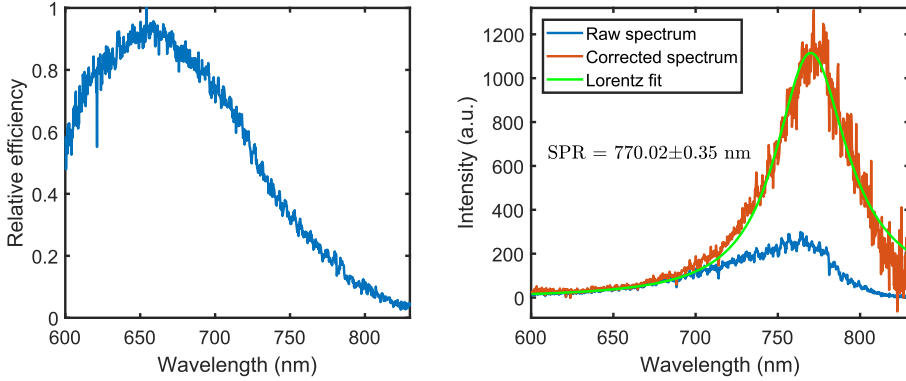


Figure S2.2: Left: Relative detection efficiency of the setup as a function of wavelength. (Right) The one-photon photoluminescence raw (blue) and corrected (red) spectra of a single nanorod. The corrected spectrum was fitted with Lorentzian line shape (green), yielding a resonance wavelength of 770.02 ± 0.35 nm.

2.5.2. Correction of gold nanorod spectra

The photoluminescence emission of gold nanorods is in the near-infrared range, where the collection efficiency of the optical setup is poor. Therefore, the measured raw spectra have to be normalized by the spectral response of the setup. To this end, we used a standard fluorophore for the near-infrared range, 4-dimethylamino-4'-nitrostillbene (4,4'-DMANS, Sigma-Aldrich), excited with the 532-nm laser. The wavelength-dependent relative detection efficiency was obtained by normalizing the measured fluorescence spectrum by the real emission spectrum of the standard dye [52]. The left panel of Fig. S2.2 shows the relative response of the setup as a function of wavelength. The measured spectra of nanorods, with the background spectra subtracted, were corrected for the spectral response function and further fitted with a Lorentzian profile to obtain the localized surface plasmon resonance wavelength. The right panel of Fig. S2.2 shows an example spectrum of a single nanorod with spectral correction and Lorentzian fitting.

2.5.3. Size of the confocal volume

We measured the size of the confocal volume by imaging gold nanorods, which are smaller than the diffraction limited point spread function (PSF) of the instrument [53]. We scanned three-dimensional photoluminescence images of a gold nanorod in water excited with the 785-nm laser. As an example, Fig. S2.3 shows the yz section of the point spread function (z is along the optical axis). All three sections (xy , xz and yz) of the point spread function were fitted with two-dimensional Gaussian functions. Taking the xy plane as an example, the model is

$$I = I_0 + I_{\max} \exp \left\{ -2 \left[\left(\frac{x - x_0}{w_x} \right)^2 + \left(\frac{y - y_0}{w_y} \right)^2 \right] \right\}. \quad (2.1)$$

(x_0, y_0) is the coordinate of the center of the section and w_x, w_y are the $1/e^2$ radii of the point spread function in the fitting plane. I_{\max} is the maximum photoluminescence intensity and I_0 is the background signal.

Table 2.1 shows the resulting lateral and axial dimensions from the fitting. The confocal volume is calculated from the mean dimensions in each axis as

$$V_{\text{conf}} = \left(\frac{\pi}{2}\right)^{3/2} w_x w_y w_z = 0.164 \pm 0.002 \text{ fL}. \quad (2.2)$$

Table 2.1: Dimensions of the point spread function determined from 2D Gaussian fits

Section	w_x / nm	w_y / nm	w_z / nm
xy	320.8 ± 4.6	275.6 ± 3.8	-
xz	326.6 ± 2.8	-	873.2 ± 7.8
yz	-	299.8 ± 2.6	912.4 ± 8.0
Mean	323.7 ± 2.7	287.7 ± 2.3	892.8 ± 5.6

2.5.4. Saturation of IRDye800CW

We measured the fluorescence intensity from the dye as a function of the excitation power to find the saturation intensity. Figure S2.4 shows the fluorescence signal from a solution of 100 nM imager-IRDye800CW in HEPES buffer as a function of the excitation power. Fluorescence scales linearly with the excitation power for power lower than $10 \mu\text{W}$. With higher power, the curve deviates from the linear relation. The fluorescence intensity decreases with increasing power for excitation power higher than $\sim 40 \mu\text{W}$, which is attributed to photobleaching. The saturation power is 5000 times higher than that is incident to the gold nanorods for the enhancement experiment. The saturation intensity is well above the local field intensity that can be achieved by the nanorods used in our study. Therefore, molecules in the close vicinity of gold nanorods are still well below saturation.

By extrapolating the data and fitting shown in Figure S2.4, we predict the fluorescence count rate to be 19.7 ± 3.1 counts/s if excited at 2 nW. For a solution of 100 nM, there are 9.9 ± 0.1 molecules in the focal volume. These yield a molecular brightness of 2.0 ± 0.3 counts/s/molecule.

2.5.5. Numerical simulations of fluorescence enhancement

Under weak excitation well below saturation (Fig. S2.4), the overall enhancement factor is the product of excitation enhancement and emission enhancement [44]. The excitation enhancement arises from the concentrated high local field due to the resonant excitation of the localized surface plasmons. The emission enhancement is a result of the competition between emission rate enhancement due to Purcell effect and fluorescence quenching due to the additional non-radiative decay pathways provided by gold.

The excitation enhancement was calculated with a finite-element method using Comsol Multiphysics. The near-field intensity map of a single gold nanorod with a size of 38 nm

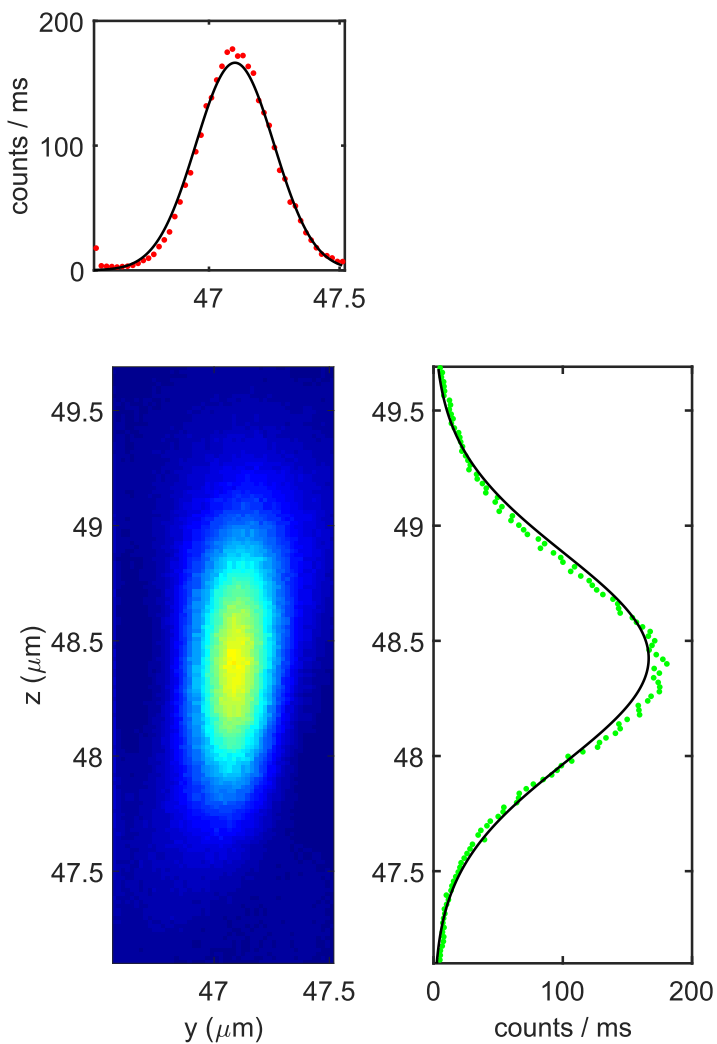


Figure S2.3: yz section of the point spread function measured with a gold nanorod. Line profiles through the center are shown. Experimental data are shown as red (along the y axis) and green (along the z axis) dots and the Gaussian fits are represented by black lines.

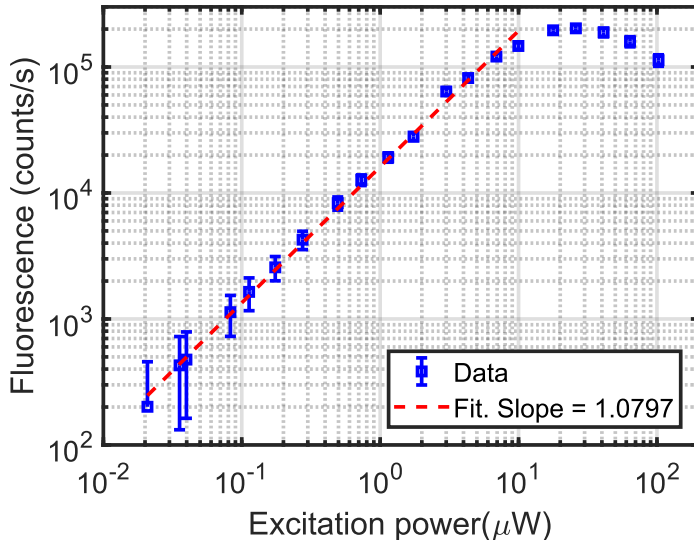


Figure S2.4: Fluorescence signal from a solution of 100 nM imager-IRDye800CW in HEPES buffer as a function of the excitation power. We found a saturation power of 10 μW .

$\times 116$ nm in water excited at 785 nm are calculated. The nanorod is found to be associated with a surface plasmon resonance at 784 nm by calculating extinction cross-sections as functions of wavelength. This size was chosen to ensure the best spectral overlap with the excitation laser and, hence, the largest enhancement factor. The incident plane wave was linearly polarized parallel to the long axis of the nanorod. The dielectric permittivity for gold was taken from Johnson and Christy[54], and the refractive index of the ambient medium was taken as 1.33. The excitation enhancement E_{exc} is the ratio of local field intensities with and without the nanorod, $E_{\text{exc}} = |\mathbf{E}|^2/|\mathbf{E}_0|^2$, at the emitter's position.

We used a boundary element method (SCUFF-EM) to evaluate the modifications of decay rates and emission enhancement using a classical electrodynamics approach [50, 51]. An IRDye800CW molecule was modeled as a radiating point dipole oscillating at a frequency which corresponds to the emission wavelength of the molecule. It was assumed that the point dipole is placed along the long axis of the nanorod with a certain distance from the tip and oriented parallel to the revolution axis of the nanorod. All the results were averaged over the actual luminescence spectrum of the molecule. The diameter and length of the nanorod were set as 38 nm and 116 nm respectively. The refractive index of the ambient medium was 1.33, and the dielectric constant for gold was taken from Johnson and Christy [54].

Figure S2.5(a) plots the modified radiative (k_r) and nonradiative (K_{nr}) decay rates relative to the intrinsic radiating rate of the dipole (k_r^0) against the separation between dipole and rod. The competition between k_r and K_{nr} leads to an emission enhancement that is represented by the green diamonds in Fig. S2.5(b). The orange triangles in Fig. S2.5 show the excitation enhancement, which is calculated by a finite-element method.

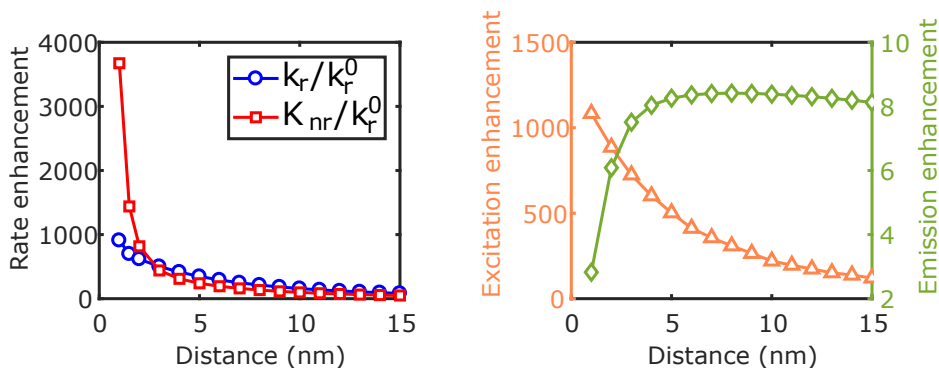


Figure S2.5: (a) Calculated radiative rate enhancement (k_r/k_r^0 , blue circles) and relative additional nonradiative rate (K_{nr}/k_r^0 , red squares) of an IRDye800CW molecule as a function of the distance to the tip of the nanorod. (b) Calculated excitation enhancement (orange triangles, left axis) and emission enhancement (green diamonds, right axis) as functions of the distance to the tip of the nanorod.

2.5.6. Calculation of nanorod temperature increase

Because the nanorods are only sparsely scattered on the substrate, bulk heating of the solution can be neglected. Each individual nanorod can be considered as an independent light-induced heat source. The local temperature increase of a nanorod depends upon the absorption cross-section, laser intensity, geometry of the nanorod, and thermal conductivities of the immersion medium and supporting substrate, as illustrated by the following equation [49]:

$$\Delta T_{NR} = \frac{\sigma_{abs} I}{4\pi R_{eq} \beta \bar{\kappa}}, \quad (2.3)$$

where σ_{abs} is absorption cross section, I intensity of illumination, R_{eq} the radius of a sphere with the same volume as the nanorod, β a nanorod geometry-dependent coefficient and $\bar{\kappa}$ the averaged thermal conductivities of water and glass.

In the calculation, we considered a nanorod with a size of $38 \text{ nm} \times 116 \text{ nm}$ by diameter and length. σ_{abs} at 785 nm was calculated using Comsol Multiphysics to be $5 \times 10^{-14} \text{ m}^2$. $I = 8.8 \text{ kW/cm}^2$ at the center of the laser focus. For a nanorod, $\beta = 1 + 0.96587 \ln^2(\text{AR}) = 2.2$ (AR is the aspect ratio of the nanorod). $\bar{\kappa} = (\kappa_{\text{water}} + \kappa_{\text{glass}})/2 = 1 \text{ W/(m}\cdot\text{K)}$. On the basis of these parameters, we calculated a temperature increase of 5.3 K at the surface of the nanorod. Such a local temperature is well below that required for thermally breaking a Au-S bond [46].

References

- [1] C. F. Bohren and D. R. Huffman, *Absorption and scattering of light by small particles* (John Wiley & Sons, 2008).
- [2] S. Link and M. A. El-Sayed, *Spectral properties and relaxation dynamics of surface*

- plasmon electronic oscillations in gold and silver nanodots and nanorods*, The Journal of Physical Chemistry B **103**, 8410 (1999).
- [3] P. Zijlstra and M. Orrit, *Single metal nanoparticles: optical detection, spectroscopy and applications*, Reports on Progress in Physics **74**, 106401 (2011).
- [4] J. R. Lakowicz, *Plasmonics in biology and plasmon-controlled fluorescence*, Plasmonics **1**, 5 (2006).
- [5] J. Pérez-Juste, I. Pastoriza-Santos, L. M. Liz-Marzán, and P. Mulvaney, *Gold nanorods: synthesis, characterization and applications*, Coordination Chemistry Reviews **249**, 1870 (2005).
- [6] L. Vigderman, B. P. Khanal, and E. R. Zubarev, *Functional gold nanorods: synthesis, self-assembly, and sensing applications*, Advanced Materials **24**, 4811 (2012).
- [7] S. Yao, H.-H. Cai, M. Liu, and P.-H. Yang, *Fluorescent labeling of cellular targets and multicolor imaging with gold nanorods*, Dyes and Pigments **101**, 286 (2014).
- [8] P. Zijlstra, P. M. Paulo, and M. Orrit, *Optical detection of single non-absorbing molecules using the surface plasmon resonance of a gold nanorod*, Nature Nanotechnology **7**, 379 (2012).
- [9] D. P. O'Neal, L. R. Hirsch, N. J. Halas, J. D. Payne, and J. L. West, *Photo-thermal tumor ablation in mice using near infrared-absorbing nanoparticles*, Cancer Letters **209**, 171 (2004).
- [10] X. Huang, I. H. El-Sayed, W. Qian, and M. A. El-Sayed, *Cancer cell imaging and photothermal therapy in the near-infrared region by using gold nanorods*, Journal of the American Chemical Society **128**, 2115 (2006).
- [11] X. Huang, P. K. Jain, I. H. El-Sayed, and M. A. El-Sayed, *Plasmonic photothermal therapy (pptt) using gold nanoparticles*, Lasers in Medical Science **23**, 217 (2008).
- [12] K. Kneipp, H. Kneipp, I. Itzkan, R. R. Dasari, and M. S. Feld, *Ultrasensitive chemical analysis by Raman spectroscopy*, Chemical Reviews **99**, 2957 (1999).
- [13] J. F. Li, Y. F. Huang, Y. Ding, Z. L. Yang, S. B. Li, X. S. Zhou, F. R. Fan, W. Zhang, Z. Y. Zhou, D. Y. Wu, B. Ren, Z. L. Wang, and Z. Q. Tian, *Shell-isolated nanoparticle-enhanced Raman spectroscopy*, Nature **464**, 392 (2010).
- [14] S. Kühn, U. Håkanson, L. Rogobete, and V. Sandoghdar, *Enhancement of single-molecule fluorescence using a gold nanoparticle as an optical nanoantenna*, Physical Review Letters **97**, 017402 (2006).
- [15] P. Anger, P. Bharadwaj, and L. Novotny, *Enhancement and quenching of single-molecule fluorescence*, Physical Review Letters **96**, 113002 (2006).
- [16] Y. Fu, J. Zhang, and J. R. Lakowicz, *Plasmonic enhancement of single-molecule fluorescence near a silver nanoparticle*, Journal of Fluorescence **17**, 811 (2007).

- [17] P. Bharadwaj, P. Anger, and L. Novotny, *Nanoplasmonic enhancement of single-molecule fluorescence*, *Nanotechnology* **18**, 044017 (2006).
- [18] J. Lakowicz and Y. Fu, *Modification of single molecule fluorescence near metallic nanostructures*, *Laser Photonics Reviews* **3**, 221 (2009).
- [19] P. Bharadwaj and L. Novotny, *Spectral dependence of single molecule fluorescence enhancement*, *Optics Express* **15**, 14266 (2007).
- [20] T. Taminiau, F. Stefani, F. B. Segerink, and N. Van Hulst, *Optical antennas direct single-molecule emission*, *Nature Photonics* **2**, 234 (2008).
- [21] M. Van Oosten, T. Schäfer, J. A. Gazendam, K. Ohlsen, E. Tsompanidou, M. C. De Goffau, H. J. Harmsen, L. M. Crane, E. Lim, K. P. Francis, *et al.*, *Real-time in vivo imaging of invasive-and biomaterial-associated bacterial infections using fluorescently labelled vancomycin*, *Nature Communications* **4**, ncomms3584 (2013).
- [22] T. Iijima, T. Aoyagi, Y. Iwao, J. Masuda, M. Fuse, N. Kobayashi, and H. Sankawa, *Cardiac output and circulating blood volume analysis by pulse dye-densitometry*, *Journal of Clinical Monitoring* **13**, 81 (1997).
- [23] R. Benson and H. Kues, *Fluorescence properties of indocyanine green as related to angiography*, *Physics in Medicine & Biology* **23**, 159 (1978).
- [24] N. Gandra, C. Portz, L. Tian, R. Tang, B. Xu, S. Achilefu, and S. Singamaneni, *Probing distance-dependent plasmon-enhanced near-infrared fluorescence using polyelectrolyte multilayers as dielectric spacers*, *Angewandte Chemie International Edition* **53**, 866 (2014).
- [25] R. Bardhan, N. K. Grady, J. R. Cole, A. Joshi, and N. J. Halas, *Fluorescence enhancement by au nanostructures: nanoshells and nanorods*, *ACS Nano* **3**, 744 (2009).
- [26] F. Tam, G. P. Goodrich, B. R. Johnson, and N. J. Halas, *Plasmonic enhancement of molecular fluorescence*, *Nano Letters* **7**, 496 (2007).
- [27] R. Bardhan, N. K. Grady, and N. J. Halas, *Nanoscale control of near-infrared fluorescence enhancement using au nanoshells*, *Small* **4**, 1716 (2008).
- [28] Y. Fu, J. Zhang, and J. R. Lakowicz, *Plasmon-enhanced fluorescence from single fluorophores end-linked to gold nanorods*, *Journal of the American Chemical Society* **132**, 5540 (2010).
- [29] H. Yuan, S. Khatua, P. Zijlstra, M. Yorulmaz, and M. Orrit, *Thousand-fold enhancement of single-molecule fluorescence near a single gold nanorod*, *Angewandte Chemie International Edition* **52**, 1217 (2013).
- [30] W. Zhang, M. Caldarola, B. Pradhan, and M. Orrit, *Gold nanorod enhanced fluorescence enables single-molecule electrochemistry of methylene blue*, *Angewandte Chemie International Edition* **56**, 3566 (2017).

- [31] B. Pradhan, S. Khatua, A. Gupta, T. Aartsma, G. Canters, and M. Orrit, *Gold-nanorod-enhanced fluorescence correlation spectroscopy of fluorophores with high quantum yield in lipid bilayers*, *Journal of Physical Chemistry C* **120**, 25996 (2016).
- [32] A. A. Kinkhabwala, Z. Yu, S. Fan, and W. E. Moerner, *Fluorescence correlation spectroscopy at high concentrations using gold bowtie nanoantennas*, *Chemical Physics* **406**, 3 (2012).
- [33] S. Khatua, H. Yuan, and M. Orrit, *Enhanced-fluorescence correlation spectroscopy at micro-molar dye concentration around a single gold nanorod*, *Physical Chemistry Chemical Physics* **17**, 21127 (2015).
- [34] A. Puchkova, C. Vietz, E. Pibiri, B. Wünsch, M. Sanz Paz, G. P. Acuña, and P. Tinnefeld, *DNA origami nanoantennas with over 5000-fold fluorescence enhancement and single-molecule detection at 25 μm* , *Nano Letters* **15**, 8354 (2015).
- [35] A. Kinkhabwala, Z. Yu, S. Fan, Y. Avlasevich, K. Müllen, and W. Moerner, *Large single-molecule fluorescence enhancements produced by a bowtie nanoantenna*, *Nature Photonics* **3**, 654 (2009).
- [36] C. Vietz, I. Kaminska, M. Sanz Paz, P. Tinnefeld, and G. P. Acuña, *Broadband fluorescence enhancement with self-assembled silver nanoparticle optical antennas*, *ACS Nano* **11**, 4969 (2017).
- [37] G. Acuna, F. Möller, P. Holzmeister, S. Beater, B. Lalkens, and P. Tinnefeld, *Fluorescence enhancement at docking sites of DNA-directed self-assembled nanoantennas*, *Science* **338**, 506 (2012).
- [38] R. Jungmann, C. Steinhauer, M. Scheible, A. Kuzyk, P. Tinnefeld, and F. C. Simmel, *Single-molecule kinetics and super-resolution microscopy by fluorescence imaging of transient binding on DNA origami*, *Nano Letters* **10**, 4756 (2010).
- [39] A. Sharonov and R. M. Hochstrasser, *Wide-field subdiffraction imaging by accumulated binding of diffusing probes*, *Proceedings of the National Academy of Sciences of the United States of America* **103**, 18911 (2006).
- [40] J. Schnitzbauer, M. T. Strauss, T. Schlichthaerle, F. Schueder, and R. Jungmann, *Super-resolution microscopy with DNA-PAINT*, *Nature Protocols* **12**, 1198 (2017).
- [41] A. Sassolas, B. D. Leca-Bouvier, and L. J. Blum, *DNA biosensors and microarrays*, *Chemical Reviews* **108**, 109 (2008).
- [42] S. Khatua and M. Orrit, *Probing, sensing, and fluorescence enhancement with single gold nanorods*, *Journal of Physical Chemistry Letters* **5**, 3000 (2014).
- [43] G. Baffou and R. Quidant, *Thermo-plasmonics: using metallic nanostructures as nano-sources of heat*, *Laser & Photonics Reviews* **7**, 171 (2013).
- [44] S. Khatua, P. M. R. Paulo, H. Yuan, A. Gupta, P. Zijlstra, and M. Orrit, *Resonant plasmonic enhancement of single-molecule fluorescence by individual gold nanorods*, *ACS Nano* **8**, 4440 (2014).

- [45] M. Yorulmaz, S. Khatua, P. Zijlstra, A. Gaiduk, and M. Orrit, *Luminescence quantum yield of single gold nanorods*, *Nano Letters* **12**, 4385 (2012).
- [46] A. M. Goodman, N. J. Hogan, S. Gottheim, C. Li, S. E. Clare, and N. J. Halas, *Understanding resonant light-triggered DNA release from plasmonic nanoparticles*, *ACS Nano* **11**, 171 (2016).
- [47] S. Simoncelli, Y. Li, E. Cortés, and S. A. Maier, *Nanoscale control of molecular self-assembly induced by plasmonic hot-electron dynamics*, *ACS Nano* **12**, 2184 (2018).
- [48] R. Huschka, J. Zuloaga, M. W. Knight, L. V. Brown, P. Nordlander, and N. J. Halas, *Light-induced release of DNA from gold nanoparticles: Nanoshells and nanorods*, *Journal of the American Chemical Society* **133**, 12247 (2011).
- [49] G. Baffou, R. Quidant, and F. J. García de Abajo, *Nanoscale control of optical heating in complex plasmonic systems*, *ACS Nano* **4**, 709 (2010).
- [50] M. T. Homer Reid and S. G. Johnson, *Efficient Computation of Power, Force, and Torque in BEM Scattering Calculations*, ArXiv e-prints (2013), "arXiv":1307.2966 ["physics.comp-ph"] .
- [51] [Http://homerreid.com/scuff-EM](http://homerreid.com/scuff-EM).
- [52] J. R. Lakowicz, *Principles of Fluorescence Spectroscopy*, 3rd ed. (Springer US, 2006) p. 954.
- [53] S. Rüttinger, V. Buschmann, B. Krämer, R. Erdmann, R. Macdonald, and F. Koberling, *Comparison and accuracy of methods to determine the confocal volume for quantitative fluorescence correlation spectroscopy*, *Journal of Microscopy* **232**, 343 (2008).
- [54] P. B. Johnson and R.-W. Christy, *Optical constants of the noble metals*, *Physical Review B* **6**, 4370 (1972).

